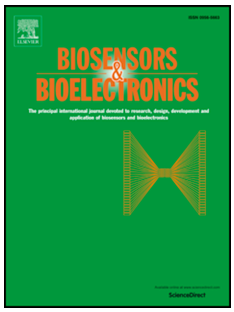

Versatile electrochemical biosensor based on bi-enzyme cascade biocatalysis spatially regulated by DNA architecture

Yongcun Yan, Zhenjie Qiao, Xin Hai, Weiling Song, Sai Bi

PII: S0956-5663(20)30813-7

DOI: https://doi.org/10.1016/j.bios.2020.112827

Reference: BIOS 112827

To appear in: *Biosensors and Bioelectronics*

Received Date: 22 September 2020

Revised Date: 10 November 2020

Accepted Date: 16 November 2020

Please cite this article as: Yan, Y., Qiao, Z., Hai, X., Song, W., Bi, S., Versatile electrochemical biosensor based on bi-enzyme cascade biocatalysis spatially regulated by DNA architecture, *Biosensors and Bioelectronics* (2020), doi: https://doi.org/10.1016/j.bios.2020.112827.

Credit Author Statement

Yongcun Yan: Investigation, Data curation, Visualization, Roles/Writing-original draft.

Zhenjie Qiao: Software, Validation.

Xin Hai: Formal analysis, Validation.

Weiling Song: Resources.

Sai Bi: Conceptualization, Funding acquisition, Methodology, Project administration, Supervision, Writing-review & editing.

Versatile electrochemical biosensor based on bi-enzyme cascade biocatalysis spatially regulated by DNA architecture

Yongcun Yan[a], Zhenjie Qiao[a], Xin Hai[a], Weiling Song[b], Sai Bi[a,*]

[a]College of Chemistry and Chemical Engineering, Research Center for Intelligent and Wearable Technology, Qingdao University, Qingdao, 266071, PR China
[b]Laboratory of Optic-electric Sensing and Analytical Chemistry for Life Science, MOE, Shandong Key Laboratory of Biochemical Analysis, Key Laboratory of Analytical Chemistry for Life Science in Universities of Shandong, College of Chemistry and Molecular Engineering, Qingdao University of Science and Technology, Qingdao 266042, P. R. China

*Corresponding author. E-mail: bisai11@126.com

ABSTRACT

The regulation of biocatalytic cascades in microenvironments for high performance and extended applications is still challenging. Herein, we develop a rolling circle amplification (RCA)-based one-pot method to prepare the micron-sized DNA flowers (DFs), which achieve the co-encapsulation and spatial regulation of bi-enzyme molecules, glucose oxidase (GOx) and horseradish peroxidase (HRP). In this system, GOx and HRP are integrated into the DFs simultaneously during RCA with the bridging of magnesium between enzyme residues and phosphate backbones on DFs. The cascade of GOx/HRP is regulated with the formation of highly ordered and hydrogen-bonded water environment in the cavity of DFs, resulting in an enhanced cascade catalytic efficiency compared with that in homogeneous solution. Moreover, the high density of DNA scaffold ensures the encapsulation of GOx/HRP with high efficiency. Accordingly, a glucose electrochemical biosensor with amplified signal response is fabricated using the as-prepared GOx/HRP DFs as biosensing interface, realizing sensitive detection of glucose. Further, through designing the complementary sequence of aptamer into the programmable circular template of RCA, the bi-enzyme co-encapsulated DFs are versatilely applied to sensitive and selective detection of cancerous exosomes and thrombin in "signal-on" and "signal-off" modes, respectively, which are further applied to the analysis of complex biological samples successfully. Overall, the encapsulation of multi-enzyme with DFs proposes a promising strategy to regulate the microenvironment of biocatalytic cascades, which hold great potential in biotechnology, bioanalysis and disease diagnosis.

Keywords: Biocatalytic cascades; Microenvironment regulation; Rolling circle amplification; DNA flowers; Electrochemical biosensor

1. Introduction

Multi-enzyme cascades play an important role in living systems, in which the ordered distribution of enzymes enables the transport of substrates to the active site in a highly efficient way (Krall and Christofk 2017; Rabe et al. 2017; Shi et al. 2018; Sweetlove and Fernie 2018). Inspired by natural ingenuity, in vitro biocatalytic cascades have been designed precisely and applied in the fields of biocatalysis (Liu et al. 2019), biosensing (Song et al. 2020), and disease treatment (Li et al. 2019a). In spite of the high reactivity and selectivity of natural enzymes, the regulation of multi-enzyme cascades in microenvironment is still required to increase the catalytic efficiency (Bilal et al. 2019; Zhang et al. 2019a). In particular, the spatial regulation of cooperating enzymes is the key to improve the cascade catalysis efficiency and stability (Agapakis et al. 2012; Booth et al. 2019; Cao et al. 2019; Li et al. 2019b). For this aim, many works have been carried out, such as the nanoclustered cascaded enzymes (Ma et al. 2019), modular enzyme assembly (Kang et al. 2019), immobilization of enzymes on micro- or nanoscale scaffolds (Hwang and Lee 2019), and so on. Among them, a variety of scaffolds, such as proteins (Liu et al. 2019), metal-organic frameworks (MOFs) (Chen et al. 2018b; Chen et al. 2018c; Wang et al. 2017b; Zhu et al. 2019), and hydrogels (Bitterwolf et al. 2019; Lilienthal et al. 2015), have been applied to spatially co-localize different kinds of enzymes for enhancing the stability and activity of the cascade (Tsitkov and Hess 2019). However, the high precision and programmable regulation of multi-enzyme cascades in large-scale operations is still a challenge.

The self-assembled DNA structures as the scaffolds is attracting growing interest because of the remarkable biocompatibility, good programmability and sensitive responsiveness of DNA building block (Fei et al. 2014; Lin et al. 2016; Meng et al. 2016). Benefiting from the progress of DNA nanotechnology, various DNA structures, such as DNA wires (Wilner et al. 2009), DNA origami triangles (Klein et al. 2019), and DNA tetrahedrons (Kong et al. 2019), have been exploited to operate the multi-enzyme cascades. However, the assembly of these structures often requires complicated design and bulky DNA preparation. In addition, the enzyme loading efficiency is often limited by the size and morphology of DNA structures. DNA flowers DFs) synthesized by rolling circle amplification (RCA) are a class of spheroidal-shaped DNA materials with three-dimensional porous structure (Chen et al. 2018a; Kim et al. 2017). Compared with the DNA structures assembled *via* complementary base pairing, the RCA-based DFs have the advantages of simple design and preparation, in which only two single-stranded DNAs (primer and circular template) are needed. Moreover, the particle sizes of the DFs can be flexibly changed from nano-scale to micron-scale through controlling the RCA reaction conditions, thus facilitating the improvement of enzyme entrapment efficiency with more binding sites (Kim et al. 2019; Liu et al. 2018). Recently, various enzymes have been encapsulated into DFs individually for bioanalysis (Kim et al. 2017), bioimaging (Hu et al. 2014), and tumor therapy (Jin et al. 2017; Pan et al. 2020; Zhang et al. 2019b). Our previous work has demonstrated that the enzymatic activity of horseradish peroxidase (HRP) could be enhanced after encapsulated into DFs through regulating

the microenvironment of DFs and the interaction between DNA scaffolds and enzyme molecules (Yan et al. 2018). To our knowledge, multi-enzyme encapsulated DFs for enhanced biocatalytic cascade has not been reported.

Herein, the micron-sized DFs are synthesized *via* RCA, which demonstrate as the advisable scaffolds for bi-enzyme cascades because of the porous structure and high loading efficiency. GOx and HRP are encapsulated into the DFs simultaneously during the liquid crystallization of polymeric DNA strands in RCA. Importantly, the catalytic activity of the cascades in DFs is enhanced compared with the enzymes in homogeneous solution. Using the as-prepared GOx/HRP DFs to modify the electrode, an electrochemical glucose biosensor has been fabricated based on the enhanced biocatalytic cascade of GOx/HRP in DFs. Moreover, given the programmability of DFs, the aptamer sequence of cancerous exosomes is readily encoded into the DFs for specific recognition of targets, resulting in the construction of a "signal-on" mode biosensor for exosome detection based on the hindrance of exosomes to the electron transport. To demonstrate the versatility of this assay, the thrombin aptamer is encoded into the DFs, which are used as the amplified labels for "signal-off" electrochemical detection of thrombin through the formation of sandwich structure of aptamer@thrombin@GOx/HRP DF on the electrode. Overall, the versatile GOx/HRP DFs-based biosensing strategies provide a new insight into sensitive and selective detection of biomolecules in bioanalysis and disease diagnosis.

2. Experimental section

Materials and reagents have been described in the Supporting information.

2.1. Preparation of circular DNA template

The primer and 5'-phosphorylated padlock probe were used to prepare the circular DNA template with the assistant of T4 DNA ligase. First, 5 μL of padlock probe (100 μM) and 10 μL of primer (100 μM) were mixed in 1× T4 DNA ligase buffer (40 mM Tris-HCl, 10 mM $MgCl_2$, 10 mM DTT, 0.5 mM ATP, pH 7.8). Then, the solution was heated at 95 °C for 5 min and slowly down to 25 °C for 3 h to ensure the hybridization of padlock probe and primer. Subsequently, 5 μL of T4 DNA ligase (5 U/μL) was added to catalyze the circularization of padlock probe at 16 °C overnight. After the inactivation of ligase at 65 °C for 10 min, the circular DNA template was formed. The residual padlock probe and primer were digested by mixing the solution with 2.5 μL of Exo I (20 U/μL) in 1× Exo I buffer (67 mM glycine-KOH, 6.7 mM $MgCl_2$, 1 mM DTT, pH 9.5) and incubated at 37 °C for 1.5 h. The Exo I was finally inactivated at 80 °C for 15 min.

2.2. Self-assembly of GOx/HRP DFs.

The GOx/HRP DFs were self-assembled *via* RCA process. The reaction was performed in a solution (33 mM Tris-acetate, 10 mM $Mg(CH_3COO)_2$, 66 mM CH_3COOK, 1% Tween 20, 1mM DTT, pH 7.9) containing GOx (24 μM), HRP (24 μM), as-prepared circular template (0.72 μM), dNTPs (2 mM) and phi29 DNA polymerase (1 U/μL) at 30 °C for 20 h. Then, the GOx/HRP DFs were separated through centrifugation at 9000*g* for 5 min, and further washed with ultrapure water for three times. The purified GOx/HRP DFs were re-dispersed in ultrapure water and stored at 4 °C until use.

2.3. Quantification of DNA and enzymes in GOx/HRP DFs

The commercial PicoGreen dsDNA Assay Kit and Bradford Protein Assay Kit were applied to quantify the DNA and enzymes in GOx/HRP DFs though the standard curve method, respectively. To obtain the standard curve of DNA, λ-DNA was chosen as the standard and diluted to 10, 20, 40, 60, 100, 150 and 200 μg/mL by TE buffer (10 mM Tris-HCl and 1 mM EDTA-2Na, pH 8.0), respectively. Then, 5 μL of λ-DNA sample was reacted with 195 μL of Picogreen reagent in dark for 2 min and the fluorescence values (λ_{ex} = 485 nm, λ_{em} = 530 nm) were recorded on a Synergy HTX multi-mode microplate reader (BioTek, USA). Similarly, BSA as the protein standard was diluted to different concentrations and 5 μL of BSA solution was mixed with 195 μL of coomassie brilliant blue at 25 °C for 5 min. The absorbance of the solution at 595 nm was recorded on the Synergy HTX multi-mode microplate reader. The above assays were repeated three times to fit standard curves. Subsequently, the GOx/HRP DFs were incubated with Picogreen reagent and coomassie brilliant blue with three replicates in the same way to quantify the amount of DNA and enzymes, respectively. The amount of GOx and HRP was calculated by subtracting the amount of protein in DFs to eliminate the effects caused by phi29 DNA polymerase and Exo I.

2.4. Cascade biocatalytic performance of DFs

The catalytic efficiency of GOx/HRP cascade in DFs was compared with that in homogeneous aqueous phase through determining the catalyzed oxidation rate of TMB. First, 2 μL of GOx/HRP DFs, 10 μL of TMB (5 mM) and 83 μL of PBS (pH 5.5) were mixed in 96-well plate. Then, 5 μL of glucose with different concentrations (0, 0.025, 0.05, 0.1, 0.2, 0.3, 0.4, and 0.5 mM) were introduced rapidly, and the time-dependent absorbance at 652 nm was monitored. Then, the absorption spectra were recorded. The data of free enzymes and their mixture with DFs were also determined as above. Finally, the kinetic parameters were obtained by plotting the Michaelis-Menten equation.

2.5. Fabrication of glucose electrochemical biosensors

Prior to the experiments, the Au electrode (2.0 mm in diameter) was carefully polished with slurries of 0.3 and 0.05 μm alumina powder and rinsed by successive sonication in ethanol and ultrapure water, respectively. Then, the electrode was treated with piranha solution (98% H_2SO_4/30% H_2O_2, 3/1, v/v) to remove the residuum, rinsed by ethanol and ultrapure water again, and finally dried with N_2. For glucose detection, 6 μL of GOx/HRP DFs was dropped on the pre-treated Au electrode and dried for 2.5 h at 4 °C to construct the electrochemical biosensing interface (GOx/HRP DFs@Au electrode). Then, the GOx/HRP DFs@Au electrode was immersed in 10 mL of PBS containing different concentrations of glucose and TMB (0.5 mM) for 5 min for differential pulse voltammetry (DPV) measurements in the range from -0.2 to 0.6 V with a step potential of 5 mV, a pulse amplitude of 25 mV and a pulse width of 25 ms.

2.6. Fabrication of "signal-on" exosome aptasensor

To achieve the detection of exosomes specifically, the padlock probe-E was used in RCA reaction to form the GOx/HRP DFs containing CD63 aptamer, which was further used to modify the Au electrode. Then, 6 μL of exosomes with different

concentrations were dropped on the GOx/HRP DFs@Au electrode for 30 min at 4 °C. The resulting electrode was washed with ultrapure water and immersed in 10 mL of PBS containing glucose (1.5 mM) and TMB (0.5 mM) for DPV detection.

2.7. Fabrication of "signal-off" thrombin dual-aptamer biosensor

For electrochemical biosensing of thrombin, sulfhydryl-modified capture probe was first activated and immobilized on the pre-treated Au electrode through Au-S bond. Briefly, 5 μL of capture probe (12 μM) and 2 μL of TCEP (3 mM) were added to 93 μL of Tris-HCl-$MgSO_4$ buffer (10 mM, pH 8.0) at room temperature for 1 h. Then, 6 μL of the activated capture probe was dropped on Au electrode and incubated for 14 h. After that, 6 μL of MCH (1 mM) was added onto the electrode surface for 1 h to remove the loosely adsorbed capture probe and block the unoccupied surface binding sites on electrode. After thoroughly rinsed with ultrapure water, the electrode was dropped with 6 μL of thrombin with different concentrations and incubated for 1 h to ensure the specific binding of capture probe and thrombin. Finally, 6 μL of GOx/HRP DFs, which were self-assembled by the padlock probe-T-based circular template, was dropped on electrode for 1 h to form the biocatalytic cascade biosensor. The electrochemical detection was carried out in 10 mL of PBS containing glucose (1.5 mM) and TMB (0.5 mM).

2.8. Electrochemical measurements

All electrochemical measurements were operated on a CHI 660E electrochemical workstation (CH instruments, China) with a conventional three-electrode system, consisting of a modified Au working electrode, a platinum wire counter electrode and an Ag/AgCl (saturated KCl) reference electrode. Cyclic voltammetry (CV) and electrochemical impedance spectroscopy (EIS) were performed in PBS containing 10 mM of $[Fe(CN)_6]^{3-/4-}$ and 0.1 M KCl as the supporting electrolyte. The CV was conducted at a scan rate of 100 mV/s in the range from -0.2 to 0.6 V. The EIS experiments were carried out with a voltage amplitude of 5 mV and a frequency range from 0.1 Hz to 100 kHz.

3. Results and Discussion

3.1. Self-assembly and characterization of GOx/HRP DFs

Fig. 1A illustrates the self-assembly process of GOx/HRP DFs *via* RCA. In brief, two single-stranded DNAs, padlock probe and primer, are designed, in which the two ends of the padlock probe are complementary to the primer. After annealing, the padlock probe is hybridized with the primer and is further circularized by T4 DNA ligase to form the circular template with the ligation of phosphorylated 5'-end and hydroxylated 3'-end. The non-circularized padlock probes and excess primers are digested by Exo I. Non-denaturing polyacrylamide gel electrophoresis (PAGE) was carried out to confirm the successful circularization of the template DNA (Fig. S1). After that, the addition of phi29 DNA polymerase and dNTPs initiates the RCA reaction in the presence of GOx and HRP. The increased concentration of polymer-like DNA strands and magnesium pyrophosphate (Mg_2PPi) lead to the nucleation and crystallization of DFs with flower-shaped and porous structural properties (Lv et al. 2015). Meanwhile, GOx and HRP are one-pot encapsulated into the DFs because of the simultaneous coordination interactions between magnesium

with DNA scaffold and protein residues.

The morphologies and sizes of the synthesized GOx/HRP DFs were first characterized by scanning electron microscope (SEM) (Fig. 1B) and transmission electron microscopy (TEM) (Fig. 1C), respectively. The liquid crystallization results in the formation of petal-like DNA structures with hierarchical pores on the periphery. The TEM image also displays the high-density core of GOx/HRP-DFs, which are composed of polymeric DNA and inorganic Mg_2PPi crystals. Satisfactorily, after encapsulation of enzymes, no significant change is observed on the morphology of the DFs. The sizes of the prepared DNA hybrids were further confirmed by dynamic light scattering (DLS), which shows the average sizes of 964.4nm for DFs and 948.23 nm for GOx/HRP DFs (Fig. S2).

The large scale and porosity of DFs make them a highly efficient carrier for encapsulating enzyme molecules. The encapsulation of GOx and HRP was first characterized by zeta potentials (Fig. 1D). Because the DNA is negatively charged, the potential of DFs was measured to be -23.91 mV. It has been reported that the isoelectric points of HRP and GOx are 7.2 and 4.2, respectively (Wang et al. 2017a; Wang et al. 2009). Therefore, as expected, after loading of negatively charged GOx (-17.79 mV) and uncharged HRP (-0.02 mV) under neutral conditions, the potential of GOx/HRP DFs was decreased to -35.05 mV. The circular dichroism (CD) spectra also confirm the successful encapsulation of GOx and HRP in DFs (Fig. S3). We further investigated the compositions of GOx/HRP DFs by scanning transmission electron microscope (STEM)-based energy dispersive X-ray spectroscopy (EDS) mapping analysis (Fig. 1E). The high-angle annular dark-field (HAADF) images show the hierarchical structure of DFs and GOx/HRP DFs, which are accorded with the above TEM results. From EDS mapping, the compositional distribution of C, O, Mg and P are uniform in DFs and GOx/HRP DFs, confirming the composition of DNA scaffold and Mg_2PPi in DFs. However, compared with DFs the elements N and S are only observed in GOx/HRP DFs, indicating the presence of GOx and HRP. The relative atomic ratios of elements to Mg (Fig. 1F) and EDS spectra (Fig. S4) also reveal the higher content of C, N, O, Fe and S in GOx/HRP DFs than DFs, which further confirm the successful encapsulation of GOx and HRP. According to the previous study, the encapsulation of GOx and HRP is mediated by the electrostatic interactions between enzymes and negatively charged DNA scaffold (Zhao et al. 2016). In addition, the magnesium could coordinate with the phosphate backbones of the DNA backbone and carboxylates of protein residues simultaneously, which thus acts as a bridge between DNAs and enzymes (Kim et al. 2017).

To evaluate the enzyme loading efficiency of DFs, the amounts of DNA and enzymes in GOx/HRP DFs were quantified by calibration curve method using commercial assay kits (Fig. S5). Considering the double-stranded configuration of DNA scaffold in DFs (Kim et al. 2019), double-stranded λ-DNA was chosen as the standard substance for the detection of DNA concentration. As shown in Fig. 1G, The DNA concentration in GOx/HRP DFs (44.21 ± 4.51 μg/mL) is almost the same as that in DFs (46.38 ± 5.76 μg/mL), suggesting that the enzymes have no significant effect on the self-assembly of DFs based on RCA. In addition, the protein concentration in

GOx/HRP DFs is calculated to be 38.93 ± 4.84 μg/mL, demonstrating the high loading efficiency of DFs.

3.2. Cascade biocatalysis of GOx/HRP encapsulated in DFs

To verify the spatial regulation of DFs to GOx and HRP, the biocatalytic efficiency of cascade was examined. The time-dependent UV-vis absorbance and corresponding UV-vis absorption spectra of TMB catalyzed by GOx/HRP DFs, free enzymes (GOx and HRP) and the mixture of free enzymes with DFs were recorded, respectively (Fig. S6). As a result, compared with the free enzymes and the mixture of free enzymes with DFs, the oxidation rate of TMB by GOx/HRP DFs was improved 2.16-fold and 1.79-fold, respectively, indicating the enhanced biocatalytic efficiency of the cascade after encapsulation. Based on the oxidation rate at different concentration of glucose, the Michaelis constant (K_m) and saturation rate (V_{max}) values for the cascade biocatalysis were derived from the Michaelis-Menten kinetics (Fig. 1H and Table 1). The K_m values of GOx/HRP almost no change after co-encapsulating in DFs, indicating that the porous DFs structure has no effect on the affinity of enzymes with the substrates. However, the bi-enzyme co-encapsulated DFs yield a ca. 2-fold higher V_{max} than the two enzymes in homogeneous aqueous phase, which confirm the enhanced cascade catalytic activity of GOx/HRP in DFs. This phenomenon can be explained as the negatively charged phosphate backbones of DNA scaffold increase the extent of hydrogen-bonded water structures and form a highly ordered, hydrogen-bonded water environment in the cavity of DNA structure (Collins et al. 2017; Zhao et al. 2016).

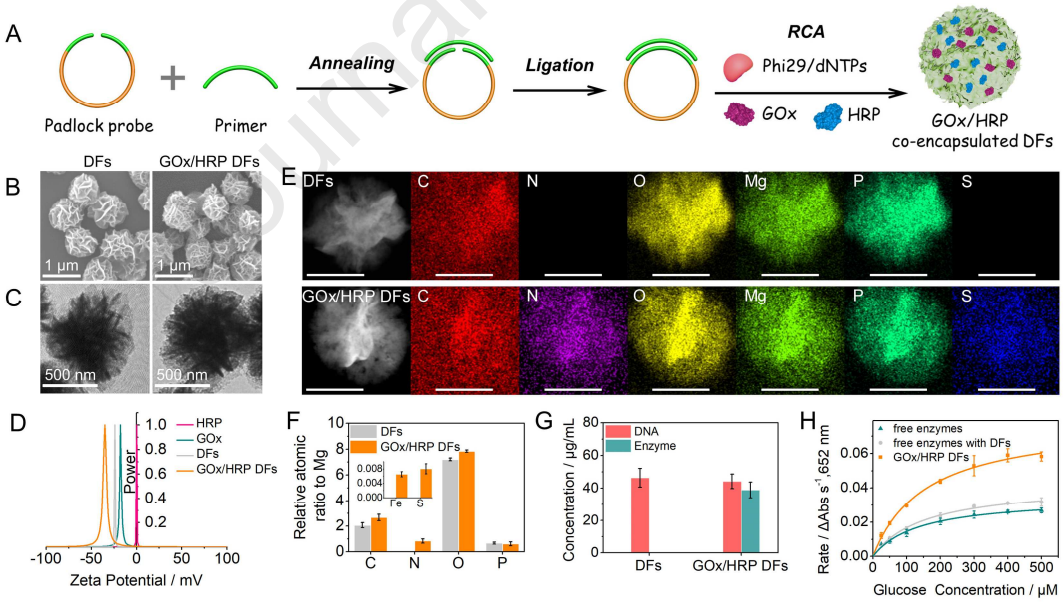

Fig. 1. Self-assembly and characterization of GOx/HRP DFs. (A) Schematic illustration of circularization of template DNA and co-encapsulation of bi-enzymes in DFs via RCA. (B) SEM and (C) TEM images of DFs and GOx/HRP DFs. (D) Zeta potentials of HRP, GOx, DFs and GOx/HRP DFs. (E) HAADF-STEM images and EDS elemental mapping of DFs and GOx/HRP DFs (scale bar: 500 nm). (F) Relative atomic ratios of C, N, O, P, Fe and S to Mg in DFs and GOx/HRP DFs, respectively. (G) The amounts of DNA and enzymes in DFs and GOx/HRP DFs, respectively. (H)

Michaelis-Menten kinetics of free enzymes (GOx and HRP), free enzymes with DFs and GOx/HRP DFs. Error bars in F, G, and H are the standard deviation of three replicate determinations.

Table 1

K_m and V_{max} values of GOx/HRP biocatalytic system in DFs compared to that in homogeneous aqueous phase.

Sample	K_m (μM)[a]	V_{max} (ΔAbs/s)[a]
GOx + HRP	138.37 ± 16.28	0.035 ± 0.0015
GOx + HRP + DFs	154.20 ± 15.52	0.043 ± 0.0016
GOx/HRP DFs	155.77 ± 14.58	0.079 ± 0.0028

[a] The results are obtained from three duplicate determinations.

3.3. Glucose electrochemical biosensor

The mechanism of biocatalytic cascade with enhanced activity for electrochemical biosensing of glucose is demonstrated in Fig. 2A. The GOx in DFs catalyzes the oxidation of glucose and the generation of H_2O_2, which further induces the oxidation of TMB immediately with the catalysis of adjacent HRP. The DPV signals are generated by the electron transport on electrode surface with the valence transformation between TMB and oxTMB, which are greatly enhanced benefitting from the high encapsulation efficiency of DFs and the microenvironment regulation of enzymes, leading to the sensitive and selective detection of glucose.

The electrocatalytic behaviors of glucose on the surface of GOx/HRP DFs@Au electrode were examined by CV and DPV, respectively (Fig. 2B). As expected, compared with bare Au electrode and free enzymes-modified Au electrode (GOx/HRP@Au electrode), the GOx/HRP DFs@Au electrode demonstrates the superior electrochemical behavior for glucose detection, which can be attributed to the high loading efficiency and enhanced cascade catalytic activity of GOx/HRP DFs. The impact of scan rate on the redox behavior of GOx/HRP DFs@Au electrode was also investigated (Fig. S7), which confirmed that the redox reaction on GOx/HRP DFs@Au electrode is a surface-controlled electrochemical process.

The GOx/HRP DFs are modified to the Au electrode surface via physical adsorption, which exhibit the favorable stability against washing step (Fig. S8). After optimizing the experimental conditions (Fig. S9), a glucose electrochemical biosensor was realized using GOx/HRP DFs as sensing interface with highly electrocatalytic activity. As presented in Fig. 2C, the absolute value of DPV signal at 0.3 V obtained from the redox of TMB demonstrates a negative correlation with the concentration of glucose. The linear relationship is ranged from 5 μM to 1.5 mM glucose with a sensitivity of 145.2 $\mu A \cdot mM^{-1} \cdot cm^{-2}$ and a limit of detection (LOD) of 3.35 μM (signal-to-noise (S/N) ratio of 3). The comparison of the present assay for glucose detection with other electrochemical glucose biosensors has been listed in Table S2, which indicate the competitive sensitivity of the present work for glucose detection. In comparison with the reported electrochemical biosensors, especially the enzymatic electrochemical biosensors, the advantages of our proposed assay for glucose

detection can be summarized as follows. (1) Easy preparation. The GOx/HRP DFs used in this study are prepared by RCA-based one-pot method, in which only two single-stranded DNAs (primer and circular template) are needed in the presence of DNA polymerase/dNTPs. (2) High sensitivity. The micron-scaled DFs with high loading capacity can provide a large number of binding sites for enzyme molecules, which thus improve the detection sensitivity. Meanwhile, the DFs have successfully performed the microenvironment regulation of the biocatalytic cascade of GOx/HRP, which enhances the cascade catalytic efficiency and results in a high sensitivity for electrochemical detection of glucose. (3) Good programmability. The DNA structures can be designed precisely through changing the base sequence, which thus not only improves the variety and specificity of GOx/HRP DFs but also achieves the versatility of this assay.

As a pivotal factor of a biosensor, the specificity of the proposed glucose electrochemical biosensor was investigated by analyzing the endogenous interfering species, including ascorbic acid (AA), uric acid (UA) and dopamine (DA). As shown in Fig. 2D, the decrease of DPV currents caused by 0.5 mM AA, UA and DA are only 6.7, 7.7 and 6.3% compared with 0.1 mM glucose, respectively, while their mixture with 0.1 mM glucose shows almost the same current response as 0.1 mM glucose. These results indicate the excellent selectivity of the biosensor for glucose detection. To further evaluate the practical performance, glucose in human blood serum was analyzed, and the results are well agreed with those obtained by the commercial glucometer with the relative standard deviation (RSD) and relative error within 4.9 and 3.11%, respectively (Table S3). These results make GOx/HRP@Au electrode a promising platform for accurate diagnosis of blood glucose level. The reproducibility of the fabricated biosensor for glucose detection was investigated by seven successive determinations toward 1.5 mM glucose with a RSD of 3.9%, confirming the good reproducibility of this electrochemical biosensing strategy.

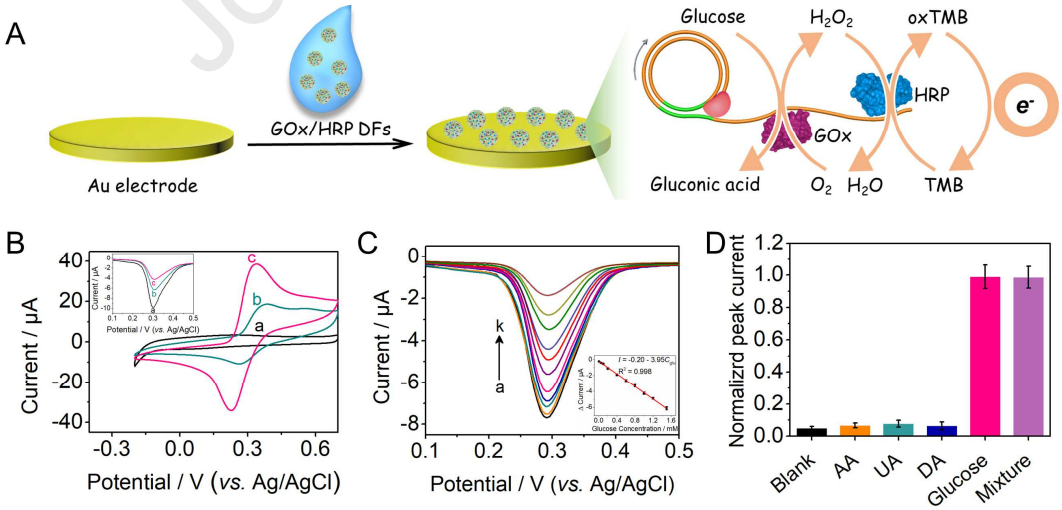

Fig. 2. Glucose electrochemical biosensor using GOx/HRP DFs as sensing interface. (A) Schematic illustration of the biosensing mechanism. (B) CV and DPV responses of (a) bare Au electrode, (b) GOx/HRP@Au electrode, and (c) GOx/HRP DFs@Au electrode in 10 mM PBS (pH 5.5) in the presence of 1.5 mM glucose and 0.5 mM

TMB. (C) DPV responses of GOx/HRP DFs@Au electrode with the glucose concentration increased from a to k (0, 0.005, 0.05, 0.1, 0.2, 0.4, 0.6, 0.8, 1.0, 1.2, 1.5 mM, respectively) in PBS (pH 5.5) in the presence of 0.5 mM TMB. Inset: calibration curve of ΔDPV current *vs* glucose concentration. (D) Normalized DPV peak current changes of the GOx/HRP DFs@Au electrode with the addition of 0.5 mM AA, 0.5 mM UA, 0.5 mM DA, 0.1 mM glucose, and their mixture. The RSDs are below 7.1%. Error bars in C and D are the standard deviation of three replicate determinations.

3.4. "Signal-on" electrochemical aptasensor for cancerous exosomes detection

Exosomes are a kind of extracellular vesicles that carry macromolecules of originating cells. Thus, the detection of cancerous exosomes has been promising in cancer diagnosis (Dong et al. 2018; He et al. 2017; Wang et al. 2017c). Fig. 3A illustrated the construction of electrochemical biosensor for exosomes detection using GOx/HRP DFs as sensing interface. Besides the porous and hierarchical structures of DFs, the programmability of DNA scaffolds further improves the variety and specificity of GOx/HRP DFs. In this work, through incorporating the complementary sequence of CD63 aptamer into the padlock probe, the GOx/HRP DFs containing large numbers of CD63 aptamers can be self-assembled after RCA reaction, which thus can specifically recognize MCF-7 exosomes. Since the exosomes with poor conductivity would block the diffusion of substrate to the GOx/HRP DFs and further inhibit the electron transport on the electrode surface, the absolute DPV signal is increasing with the increase of exosome concentration. Therefore, the exosomes can be quantified in a "signal-on" mode.

First, the morphology and size distribution of the purified MCF-7 exosomes were examined by TEM and Nanoparticle Tracking Analysis (NTA), respectively (Fig. 3B). The MCF-7 exosomes are nanoscale globoid vesicles with the size distribution of ~110 nm and particle concentration of 1.78×10^9 particles/mL. To verify the feasibility of this aptasensor for exosomes detection, the CV and EIS of the electrodes were recorded during the assembly process using $[Fe(CN)_6]^{3-/4-}$ as electroactive probe (Fig. 3C). For CV measurement, compared with the bare Au electrode, the peak current of GOx/HRP DFs@Au electrode decreases, showing the electronically inert feature of GOx/HRP DFs. After the capture of exosomes, the peak current further decreases because of the hinderance of the GOx/HRP cascade on the electrode by exosomes. In addition, the electron transfer resistance (R_{et}) of the electrode at different stages measured by EIS shows a good agreement with CV results, confirming the successful conjugation between GOx/HRP DFs and exosomes. The equivalent circuit fitting with the obtained EIS spectra is shown in Fig. S10 and the fitting values of the equivalent circuit elements are listed in Table S4. In addition, the specific binding of GOx/HRP DFs and exosomes was also confirmed by zeta potentials (Fig. S11).

Since the aptamer sequence can be greatly replicated *via* RCA, the resulting aptamer-incorporated GOx/HRP DFs can specially bind with exosomes in a high ratio, which thus results in the fabrication of "signal-on" electrochemical biosensor for exosomes detection (Fig. S12). From Fig. 3D, after the reaction of MCF-7 exosomes

with GOx/HRP DFs@Au electrode, the absolute DPV peak current at 0.3 V increases proportionally with increasing the concentration of exosomes from 1.5 × 10^3 to 1.3 × 10^5 particles/μL. The LOD is calculated as 1.02 × 10^3 particles/μL (S/N ratio of 3). Compared to the previous methods for exosomes detection (Wang et al. 2017d; Zhang et al. 2018), the proposed biosensor was simple and rapid, which can be finished within 35 min. To investigate the specificity of the proposed aptasensor, the DPV responses generated by nontumorigenic cell line (MCF-10A) exosomes and human ovarian cancer cell (OVCAR-3) exosomes with the same concentration (1.0 × 10^5 particles/μL) as MCF-7 exosomes were monitored (Fig. 3E). The largest DPV change was obtained by MCF-7 exosomes, while the DPV change caused by MCF-10A and OVCAR-3 is much smaller. The good selectivity can be attributed to the high expression level of CD63 on MCF-7 exosomes (Wang et al. 2017d; Xia et al. 2017; Yoshioka et al. 2013), which results in the specific recognition of MCF-7 exosomes with aptamers in GOx/HRP DFs on the electrode. To evaluate the clinical application of this biosensor, we quantified the MCF-7 exosomes with different concentrations in diluted human serum samples (Table S5). The acceptable recoveries (from 94% to 104%) and RSDs (from 4.9% to 8.2%) demonstrate that the as-prepared aptasensor can be readily applied to tumor exosomes analysis in real samples. What's more, seven independently prepared GOx/HRP DFs@Au electrodes for exosome detection result in a RSD of 4.5%, showing the excellent reproducibility of this electrochemical aptasensor.

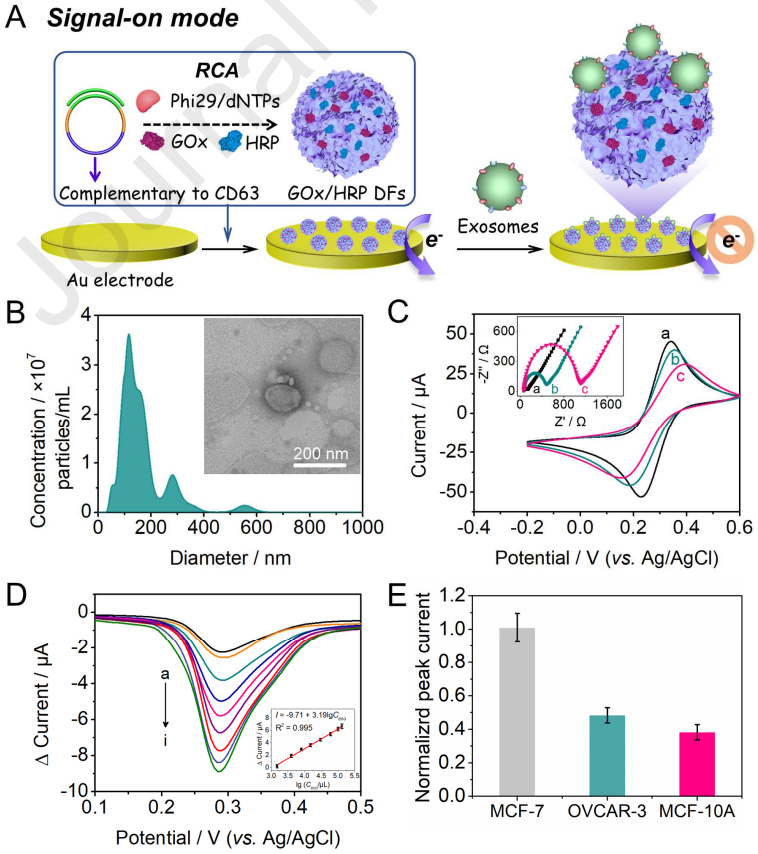

Fig. 3. "Signal-on" electrochemical exosomes aptasensor using CD63-incorporated GOx/HRP DFs as sensing interface and specific recognition element. (A) Schematic

illustration of the biosensing mechanism. (B) TEM images and NTA analysis of MCF-7 exosomes. (C) CV and EIS responses of (a) bare Au electrode, (b) GOx/HRP DFs@Au electrode, and (c) exosomes@GOx/HRP DFs@Au electrode in 10 mM $[Fe(CN)_6]^{3-/4-}$. (D) DPV responses of GOx/HRP DFs@Au electrode with exosomes concentration increased from a to i (0, 1 500, 4 000, 8 000, 15 000, 30 000, 60 000, 100 000, and 130 000 particles/μL) in PBS (pH 5.5) in the presence of 1.5 mM glucose and 0.5 mM TMB. Inset: calibration curve of ΔDPV currents *vs* logarithm of exosomes concentrations. (E) Selectivity of the aptasensor for MCF-7 exosomes against MCF-10A exosomes and OVCAR-3 exosomes. The RSDs are below 8.5%. Error bars are the standard deviation of three replicate determinations.

3.5. "Signal-off" electrochemical dual-aptamer biosensor for thrombin detection

The fabrication of dual-aptamer recognition-based electrochemical thrombin biosensor is illustrated in Fig. 4A. In this assay, the complementary sequence of thrombin aptamer (Apt29) is designed in the circular template, which results in the self-assembly of repeated aptamers-decorated DFs and thus simultaneously realizes the biocatalytic cascade and specific recognition of GOx/HRP DFs to thrombin. Meanwhile, the capture probe containing another thrombin aptamer (Apt15) is immobilized on the electrode surface through Au-S bond to recognize and conjugate thrombin with high affinity and specificity. The loosely adsorbed capture probe and the unoccupied binding sites on the electrode are eliminated by MCH. After thrombin is specifically caught by the capture probe, the electrode is further incubated with GOx/HRP DFs to form the sandwich structure of Apt15@thrombin@GOx/HRP DFs based on the specific binding of thrombin with two aptamers. The "signal-off" electrochemical signal recorded in glucose solution is related to the thrombin concentration. In particular, the signal is amplified by the enhanced activity of the biocatalytic cascade and high encapsulation efficiency of DFs, thus improving the sensitivity for thrombin analysis.

CV and EIS were used to characterize the assembly process of the electrode. From the CV results (Fig. 4B), the redox peaks altered gradually with the sequential modification of capture probe, MCH, thrombin, and GOx/HRP DFs. In brief, the bare Au electrode shows a high oxidation peak current of 53.78 μA (curve a) due to the formation of polished surface after pretreatment. After the capture probe are immobilized onto the electrode, the oxidation peak current decreases to 45.42 μA (curve b), which can be attributed to the poor conductivity of the probe. Moreover, the current decreases to 35.20 μA (curve c) after blocking the unmodified sites by MCH. The specific binding of thrombin (curve d) and subsequent GOx/HRP DFs (curve e) further cause the decreased peak currents, which can be attributed to the poor conductivity of thrombin and bi-enzyme co-encapsulated DFs to inhibit the penetration of redox probe and electron transport. The binding affinity of Apt29 in GOx/HRP DFs with thrombin was verified through fitting the Hill-Langmuir equation that describes the equilibrium binding (Khan et al. 2020) (Fig. S13). The equilibrium dissociation constant (K_D) was estimated to be 1.44 nM, which is only 3-fold to that of the original aptamer reported previously (0.5 nM) (Tasset et al. 1997). Therefore,

there is almost no effect on the binding affinity of aptamers into the DFs. In addition, EIS results also prove the successful fabrication of this aptasensor, in which the R_{et} of the electrode gradually increases with the sequential modification (Fig. 4C).

Under the optimized conditions (Fig. S14), the analytical performance of the dual-aptamer biosensor for thrombin detection was investigated. As shown in Fig. 4D, since more thrombin can bind more GOx/HRP DFs on the electrode, the absolute DPV currents decrease obviously with the increase of thrombin concentration. The linear calibration plot shows that the ΔDPV currents exhibit a good linear relationship with the logarithm of thrombin concentration ranging from 15 fM to 1×10^{-7} M, and the LOD is calculated to be 12.77 fM (S/N ratio of 3). The specificity of the dual-aptamer biosensor was further examined (Fig. 4E). As expected, almost no signal response is recorded to the interferents, including bovine serum albumin (BSA), cysteine (Cys) and lysozyme (Lys), even the concentration is 5-fold higher than thrombin. The high specificity can be attributed to the specific recognition of thrombin with two aptamers. The practical application of the biosensor was investigated in diluted human blood serum by standard addition method (Table S6). The analytical recoveries ranging from 96.2 to 104.7% with the RSD within 7.0% indicate that the proposed dual-aptamer biosensor is capable to thrombin detection in real samples. Seven thrombin determinations using independently prepared electrodes show a RSD of 4.9%, which indicate the good reproducibility of the proposed dual-aptamer biosensor.

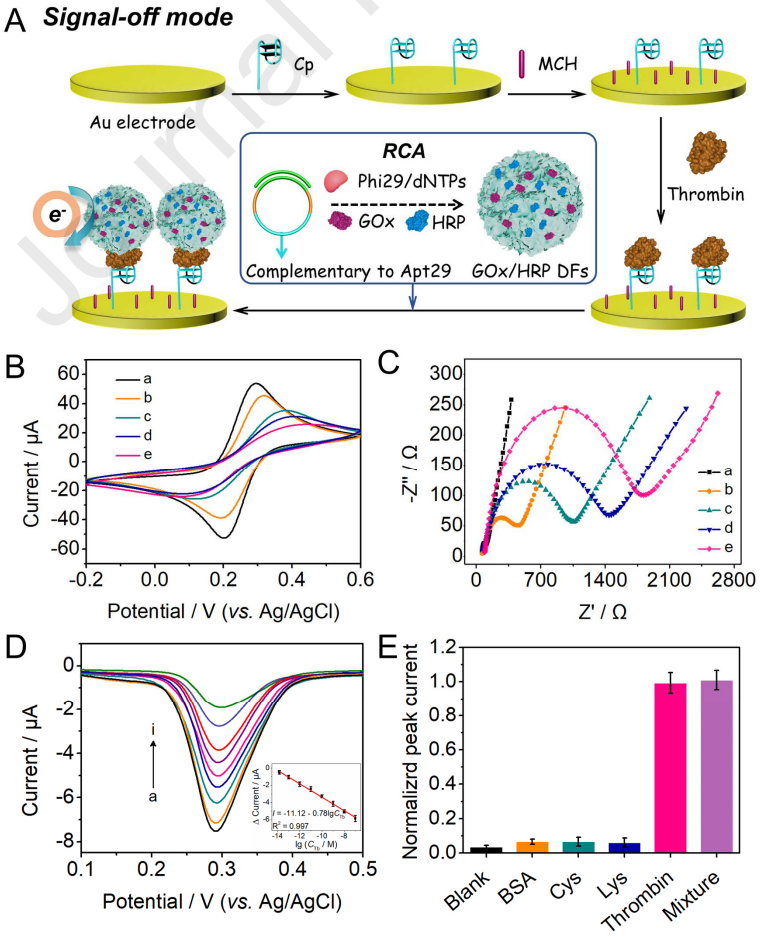

Fig. 4. "Signal-off" electrochemical dual-aptamer biosensor for thrombin detection using Apt15 as capture probe and Apt29-incorporated GOx/HRP DFs as amplified labels. (A) Schematic illustration of the biosensing mechanism. (B) CV and (C) EIS responses of (a) bare Au electrode, (b) capture probe (Cp)@Au electrode, (c) MCH@Cp@Au electrode, (d) thrombin@MCH@Cp@Au electrode, (e) GOx/HRP DFs@thrombin@MCH@Cp@Au electrode in 10 mM $[Fe(CN)_6]^{3-/4-}$. (D) DPV responses of the biosensor with the thrombin concentration increased from a to i (0, 1.5×10^{-14}, 1×10^{-13}, 1×10^{-12}, 1×10^{-11}, 1×10^{-10}, 1×10^{-9}, 1×10^{-8}, and 1×10^{-7} M) in PBS (pH 5.5) in the presence of 1.5 mM glucose and 0.5 mM TMB. Inset: calibration curve of ΔDPV currents *vs* logarithm of thrombin concentrations. (E) The selectivity toward thrombin (20 fM) from 100 fM BSA, 100 fM Cys, 100 fM Lys, and their mixture with 20 fM thrombin. The RSDs are below 6.0%. Error bars in D and E are the standard deviation of three replicate determinations.

4. Conclusion

In summary, we have developed a bi-enzyme co-encapsulated DNA flower structure *via* RCA, achieving an enhanced cascade biocatalysis and versatile fabrication of electrochemical biosensors. The RCA-based DFs have demonstrated the unique characteristics of porous and hierarchical structure, favorable programmability, high loading efficiency and good biocompatibility. The one-pot encapsulation of GOx and HRP into DFs realizes the programmable and spatial regulation of bi-enzyme molecules in micron scale. Meanwhile, the DFs successfully perform the microenvironment regulation of the biocatalytic cascade of GOx/HRP, which enhance the cascade catalytic efficiency by ca. 2-fold compared with that in homogeneous aqueous phase. Using the GOx/HRP DFs as excellent sensing interface, a glucose electrochemical biosensor is readily constructed, achieving a LOD as low as 3.35 μM. Moreover, the electrochemical aptasensors are proposed by encoding aptamer sequences into the DFs, which are used as sensing interface and amplified labels for "signal-on" and "signal-off" detection of cancerous exosomes and thrombin, achieving the LODs of 1.02×10^3 particles/μL and 12.77 fM, respectively. Therefore, our proposed strategy of RCA-based multi-enzyme encapsulated DFs with space and microenvironment regulation opens a promising avenue to design biocatalytic cascades, which further offers a powerful tool for the development of DNA nanotechnology and biosensing platforms.

Acknowledgment

The authors greatfully appreciate the support from the National Natural Science Foundation of China (21722505 and 22076087), the Special Funds of the Taishan Scholar Program of Shandong Province (tsqn20161028), the Youth Innovation Technology Program of Shandong Province (2019KJC029), the Collaborative Innovation Program of Jinan (2018GXRC033), and the Open Project of Chemistry Department of Qingdao University of Science and Technology (QUSTHX201928).

Appendix A. Supplementary material

Supplementary data associated with this article can be found in the online version at http://dx.doi.org/

References

Agapakis, C.M., Boyle, P.M., Silver, P.A., 2012. Nat. Chem. Biol. 8(6), 527-535.

Bilal, M., Cui, J., Iqbal, H.M.N., 2019. Int. J. Biol. Macromol. 130, 186-196.

Bitterwolf, P., Gallus, S., Peschke, T., Mittmann, E., Oelschlaeger, C., Willenbacher, N., Rabe, K.S., Niemeyer, C.M., 2019. Chem. Sci. 10(42), 9752-9757.

Booth, R., Qiao, Y., Li, M., Mann, S., 2019. Angew. Chem. Int. Ed. Engl. 58(27), 9120-9124.

Cao, Y., Li, X., Xiong, J., Wang, L., Yan, L.T., Ge, J., 2019. Nanoscale 11(45), 22108-22117.

Chen, J., Baker, Y.R., Brown, A., El-Sagheer, A.H., Brown, T., 2018a. Chem. Sci. 9(42), 8110-8120.

Chen, W.-H., Vázquez-González, M., Zoabi, A., Abu-Reziq, R., Willner, I., 2018b. Nat. Catal. 1(9), 689-695.

Chen, W.H., Luo, G.F., Vazquez-Gonzalez, M., Cazelles, R., Sohn, Y.S., Nechushtai, R., Mandel, Y., Willner, I., 2018c. ACS Nano 12(8), 7538-7545.

Collins, J., Zhang, T., Oh, S.W., Maloney, R., Fu, J., 2017. Chem. Commun. 53(97), 13059-13062.

Dong, H., Chen, H., Jiang, J., Zhang, H., Cai, C., Shen, Q., 2018. Anal. Chem. 90(7), 4507-4513.

Fei, Z., Jeanette, N., Yan, L., Hao, Y., 2014. J. Am. Chem. Soc. 136(32), 11198-11211.

He, F., Liu, H., Guo, X., Yin, B.-C., Ye, B.-C., 2017. Anal. Chem. 89(23), 12968-12975.

Hu, R., Zhang, X., Zhao, Z., Zhu, G., Chen, T., Fu, T., Tan, W., 2014. Angew. Chem. Int. Ed. Engl. 53(23), 5821-5826.

Hwang, E.T., Lee, S., 2019. ACS Catal. 9(5), 4402-4425.

Jin, Y., Li, Z., Liu, H., Chen, S., Wang, F., Wang, L., Li, N., Ge, K., Yang, X., Liang, X.-J., Zhang, J., 2017. NPG Asia Mater. 9(3), e365-e365.

Kang, W., Ma, T., Liu, M., Qu, J., Liu, Z., Zhang, H., Shi, B., Fu, S., Ma, J., Lai, L.T.F., He, S., Qu, J., Wing-Ngor Au, S., Ho Kang, B., Yu Lau, W.C., Deng, Z., Xia, J., Liu, T., 2019. Nat. Commun. 10(1), 4248.

Khan, N.I., Mousazadehkasin, M., Ghosh, S., Tsavalas, J.G., Song, E., 2020. Analyst 145(13), 4494-4503.

Kim, E., Agarwal, S., Kim, N., Hage, F.S., Leonardo, V., Gelmi, A., Stevens, M.M., 2019. ACS Nano 13(3), 2888-2900.

Kim, E., Zwi-Dantsis, L., Reznikov, N., Hansel, C.S., Agarwal, S., Stevens, M.M., 2017. Adv. Mater. 29(26), 1701086.

Klein, W.P., Thomsen, R.P., Turner, K.B., Walper, S.A., Vranish, J., Kjems, J., Ancona, M.G., Medintz, I.L., 2019. ACS Nano 13(12), 13677-13689.

Kong, L., Wang, D., Chai, Y., Yuan, Y., Yuan, R., 2019. Anal. Chem. 91(15), 10289-10294.

Krall, A.S., Christofk, H.R., 2017. Nature 546(7658), 357-358.

Li, H., Li, Q., Hou, W., Zhang, J., Yu, C., Zeng, D., Liu, G., Li, F., 2019a. ACS Appl. Mater. Interfaces 11(46), 43581-43587.

Li, J., Liu, X., Abdelmohsen, L., Williams, D.S., Huang, X., 2019b. Small 15(36), e1902893.

Lilienthal, S., Shpilt, Z., Wang, F., Orbach, R., Willner, I., 2015. ACS Appl. Mater. Interfaces 7(16), 8923-8931.

Lin, M., Song, P., Zhou, G., Zuo, X., Aldalbahi, A., Lou, X., Shi, J., Fan, C., 2016. Nat. Protoc. 11(7), 1244-1263.

Liu, M., Zhang, Q., Kannan, B., Botton, G.A., Yang, J., Soleymani, L., Brennan, J.D., Li, Y., 2018. Angew. Chem. Int. Ed. Engl. 57(38), 12440-12443.

Liu, Z., Cao, S., Liu, M., Kang, W., Xia, J., 2019. ACS Nano 13(10), 11343-11352.
Lv, Y., Hu, R., Zhu, G., Zhang, X., Mei, L., Liu, Q., Qiu, L., Wu, C., Tan, W., 2015. Nat. Protoc. 10(10), 1508-1524.
Ma, Y., Zhao, Y., Bejjanki, N.K., Tang, X., Jiang, W., Dou, J., Khan, M.I., Wang, Q., Xia, J., Liu, H., You, Y.Z., Zhang, G., Wang, Y., Wang, J., 2019. ACS Nano 13(8), 8890-8902.
Meng, H.-M., Liu, H., Kuai, H., Peng, R., Mo, L., Zhang, X.-B., 2016. Chem. Soc. Rev. 45(9), 2583-2602.
Pan, M., Jiang, Q., Sun, J., Xu, Z., Zhou, Y., Zhang, L., Liu, X., 2020. Angew. Chem. Int. Ed. Engl. 59(5), 1897-1905.
Rabe, K.S., Müller, J., Skoupi, M., Niemeyer, C.M., 2017. Angew. Chem. Int. Ed. 56(44), 13574-13589.
Shi, J., Wu, Y., Zhang, S., Tian, Y., Yang, D., Jiang, Z., 2018. Chem. Soc. Rev. 47(12), 4295-4313.
Song, P., Shen, J., Ye, D., Dong, B., Wang, F., Pei, H., Wang, J., Shi, J., Wang, L., Xue, W., Huang, Y., Huang, G., Zuo, X., Fan, C., 2020. Nat. Commun. 11(1), 838.
Sweetlove, L.J., Fernie, A.R., 2018. Nat. Commun. 9(1), 2136.
Tasset, D.M., Kubik, M.F., Steiner, W., 1997. J. Mol. Biol. 272(5), 688-698.
Tsitkov, S., Hess, H., 2019. ACS Catal. 9(3), 2432-2439.
Wang, C., Luo, X., Jia, Z., Shi, Q., Zhu, R., 2017a. Appl. Surf. Sci. 406, 170-177.
Wang, Q., Zhang, X., Huang, L., Zhang, Z., Dong, S., 2017b. Angew. Chem. Int. Ed. Engl. 56(50), 16082-16085.
Wang, S., Zhang, L., Wan, S., Cansiz, S., Cui, C., Liu, Y., Cai, R., Hong, C., Teng, I.T., Shi, M., Wu, Y., Dong, Y., Tan, W., 2017c. ACS Nano 11(4), 3943-3949.
Wang, Y.M., Liu, J.W., Adkins, G.B., Shen, W., Trinh, M.P., Duan, L.Y., Jiang, J.H., Zhong, W., 2017d. Anal. Chem. 89(22), 12327-12333.
Wang, Y.-T., Yu, L., Zhu, Z.-Q., Zhang, J., Zhu, J.-Z., Fan, C.-h., 2009. Sens. Actuators, B 136(2), 332-337.
Wilner, O.I., Shimron, S., Weizmann, Y., Wang, Z.-G., Willner, I., 2009. Nano Lett. 9(5), 2040-2043.
Xia, Y., Liu, M., Wang, L., Yan, A., He, W., Chen, M., Lan, J., Xu, J., Guan, L., Chen, J., 2017. Biosens. Bioelectron. 92, 8-15.
Yan, Y., Li, J., Li, W., Wang, Y., Song, W., Bi, S., 2018. Nanoscale 10(47), 22456-22465.
Yoshioka, Y., Konishi, Y., Kosaka, N., Katsuda, T., Kato, T., Ochiya, T., 2013. J. Extracell. Vesicles 2(1), 20424.
Zhang, H., Zhang, H., Luo, J., Wan, Y., 2019a. ACS Appl. Mater. Interfaces 11(25), 22419-22428.
Zhang, J.L., Shi, J.J., Liu, W., Zhang, K.X., Zhao, H.J., Zhang, H.L., Zhang, Z.Z., 2018. Sens. Actuators, B 276, 552-559.
Zhang, L., Abdullah, R., Hu, X., Bai, H., Fan, H., He, L., Liang, H., Zou, J., Liu, Y., Sun, Y., Zhang, X., Tan, W., 2019b. J. Am. Chem. Soc. 141(10), 4282-4290.
Zhao, Z., Fu, J., Dhakal, S., Johnson-Buck, A., Liu, M., Zhang, T., Woodbury, N.W., Liu, Y., Walter, N.G., Yan, H., 2016. Nat. Commun. 7, 10619.
Zhu, D., Ao, S., Deng, H., Wang, M., Qin, C., Zhang, J., Jia, Y., Ye, P., Ni, H., 2019. ACS Appl. Mater. Interfaces 11(37), 33581-33588.

Highlights

- A rolling circle amplification-based one-pot method is developed to prepare DNA flowers (DFs).
- An enhanced cascade biocatalysis of GOx/HRP is regulated in highly ordered DFs with hydrogen-bonded water environment.
- GOx/HRP DFs are versatilely applied to fabricate electrochemical biosensors with signal amplification.
- Successful analysis of complex biological samples is demonstrated.

Declaration of interests

☒ The authors declare that they have no known competing financial interests or personal relationships that could have appeared to influence the work reported in this paper.

☐The authors declare the following financial interests/personal relationships which may be considered as potential competing interests: